

INF³: Implicit Neural Feature Fusion Function for Multispectral and Hyperspectral Image Fusion

ShangQi Deng*

RuoCheng Wu*

shangqideng0124@gmail

School of Mathematical Sciences, University of Electronic
Science and Technology of China
Chengdu, China

Ran Ran

RanRan@std.uestc.edu.cn

School of Mathematical Sciences, University of Electronic
Science and Technology of China
Chengdu, China

Liang-Jian Deng[†]

liangjian.deng@uestc.edu.cn

School of Mathematical Sciences, University of Electronic
Science and Technology of China
Chengdu, China

Tai-Xiang Jiang

taixiangjiang@gmail.com

Southwestern University of Finance and Economics
Chengdu, China

ABSTRACT

Multispectral and Hyperspectral Image Fusion (MHIF) is a practical task that aims to fuse a high-resolution multispectral image (HR-MSI) and a low-resolution hyperspectral image (LR-HSI) of the same scene to obtain a high-resolution hyperspectral image (HR-HSI). Benefiting from powerful inductive bias capability, CNN-based methods have achieved great success in the MHIF task. However, they lack certain interpretability and require convolution structures be stacked to enhance performance. Recently, Implicit Neural Representation (INR) has achieved good performance and interpretability in 2D tasks due to its ability to locally interpolate samples and utilize multimodal content such as pixels and coordinates. Although INR-based approaches show promise, they require extra construction of high-frequency information (e.g., positional encoding). In this paper, inspired by previous work of MHIF task, we realize that HR-MSI could serve as a high-frequency detail auxiliary input, leading us to propose a novel INR-based hyperspectral fusion function named Implicit Neural Feature Fusion Function (INF³). As an elaborate structure, it solves the MHIF task and addresses deficiencies in the INR-based approaches. Specifically, our INF³ designs a Dual High-Frequency Fusion (DHFF) structure that obtains high-frequency information twice from HR-MSI and LR-HSI, then subtly fuses them with coordinate information. Moreover, the proposed INF³ incorporates a parameter-free method named INR with cosine similarity (INR-CS) that uses cosine similarity to generate local weights through feature vectors. Based on INF³, we construct an Implicit Neural Fusion Network (INFN) that achieves state-of-the-art performance for MHIF tasks of two public datasets, *i.e.*, CAVE and Harvard. The code will soon be made available on GitHub.

KEYWORDS

Implicit Neural Representation (INR), Multispectral and Hyperspectral Image Fusion (MHIF)

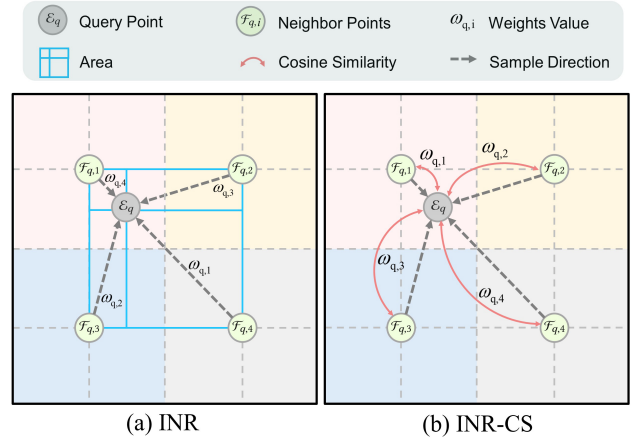


Figure 1: (a) The left figure shows the INR of generating weights based on area in LIIF [2]. (b) The proposed INR with cosine similarity (INR-CS) method, which generates weights based on cosine similarity and takes into account the pixel values, is depicted in the right figure. Our method generates more reasonable weights by taking into account the correlation of points in the feature space, in contrast to LIIF-generated weights that consider only relative positions in the coordinate space.

1 INTRODUCTION

Hyperspectral imaging involves capturing a scene in various contiguous spectral bands. Compared to traditional single or few-band images (such as those with RGB channels), hyperspectral (HS) images provide finer information about real observations and thus better characterize image scenes. As a result, HSIs have found wide application in different areas of computer vision and have improved the accuracy of several tasks, such as object recognition, classification, tracking, and segmentation [7, 29–31]. However, practical

*Both authors contributed equally to this research.

[†]Corresponding author

optical sensor systems face limitations in incident energy, necessitating tradeoffs between spatial resolution and spectral refinement. In particular, hyperspectral (HS) images with more than 100 bands often have a relatively low spatial resolution, while multispectral (MS) images with a limited number of bands have a relatively high spatial resolution. Therefore, exploring the fusion of a high spatial resolution multispectral image (HR-MSI) and a low spatial resolution hyperspectral image (LR-HSI) of the same scenario into a high spatial resolution hyperspectral image (HR-HSI) has attracted increasing attention. The aim is to obtain as rich and precise HR and HS data as possible.

In recent times, the CNN-based method has achieved considerable success due to its remarkable ability to extract advanced features when applied to multispectral and hyperspectral image fusion. Researchers have demonstrated that the two-stream fusion network designed for HR-MSI and MR-HSI is bounded by the two-stream fusion network for them. To maintain both spatial and spectral information, existing work attempts to design attention modules that produce high-quality spatial details. However, most existing networks are based on a generic CNN framework, which lacks interpretability for MHIF tasks.

Motivated by recent advancements in Implicit Neural Representation (INR) for 3D object/scene representation [12, 18, 20] and image super-resolution [2, 28, 37], we propose to re-examine the fusion process from a different perspective. INR involves mapping continuous spatial coordinates to signals in a domain through an implicit function. In order to obtain prior information from different scenes and integrate it with the implicit function, an existing encoder is typically employed to extract the latent code from the scene/imagery. For 2D tasks, the implicit function usually takes a weighted average of a fixed number of neighboring latent codes to ensure output value continuity. However, due to the lack of sufficient prior information across neighboring coordinates, the weights of such implicit interpolation are commonly dependent on area [2] or network parameters [28], which limit performance or interpretability. Thus we generate fusion weights using parameter-free cosine similarity solving of the latent code. Additionally, the MLP-ReLU structure used by INR has inherent high-frequency information bias [21] that is not easily eliminated during training. Therefore, we propose aligning HR-MSI and LR-HSI images to extract high-frequency information in a multiscale and multimodal manner. Finally, we integrate the learning framework of weight generation and image fusion into a unified implicit function, called the implicit neural feature fusion function (INF³) representation.

The contribution of this paper is listed as follows:

- We propose an Implicit Neural Feature Fusion Function (INF³), which is the first attempt that applied Implicit Neural Representation (INR) on Multispectral and Hyperspectral Image Fusion (MHIF) task. In the fusion stage, we only utilize an MLP layer, which reduces the burden brought by massive use of convolution.
- To enrich the network's input, our INF³ adopts the practice of Dual High-Frequency Fusion (DHFF) structure across three modalities which combines high-frequency spatial information at different resolutions. Concretely, this method

allows the MLP layer in INF³ to access more high-frequency information for detail recovery.

- The proposed INR with cosine similarity (INR-CS) method utilizes cosine similarity to generate weights that makes better use of information inside the pixel rather than distance or area. The proposed method does not depend on any extra parameters or network structures. Instead, it generates parameters based on cosine similarity between feature vectors and fuses local information.
- Based upon INF³, we construct an Implicit Neural Fusion Network (INFN) using encoder-decoder architecture. The proposed INFN has achieved state-of-the-art performance on two public datasets, *i.e.*, CAVE and Harvard. Specifically, the proposed decoder has a lightweight structure yet prevents overfitting of INR structures on MHIF tasks.

2 RELATED WORK

2.1 CNNs in MHIF

Recently, CNN-based techniques have shown significant success in multispectral and hyperspectral image fusion (MHIF) due to their capacity to learn high-level features from input data through end-to-end training. Among these methods, SSRNet [38] uses three convolution modules—fusion, spatial edge, and spectral edge—to restructure the image, with a loss function connected to the spatial and spectral edges ensuring training reliability. Similarly, ResTFNet [16] utilizes residual structures and a two-stream fusion network to learn input data from different modalities, inspired by the widespread application of ResNet [8] in image super-resolution. MHF-net [34], on the other hand, was specifically designed for the MS/HS fusion task, incorporating a well-researched linear mapping that links the HR-HSI image to the HR-MSI and LR-HSI images, as well as clear interpretability. Meanwhile, MoG-DCN [6] builds a dedicated sub-network for approximating the degradation matrix and leverages DCN-based image regularization [5] for HISR, fully exploiting prior HSI knowledge. For simultaneous extraction of spatial and spectral information and production of high-quality details, HSRnet [10] employs channel and spatial attention modules. To ensure bidirectional data consistency and improve accuracy in both spatial and spectral domains, DBIN [32] proposes a deep learning-based approach that optimizes the observation model and fusion procedures repeatedly and alternately during reconstruction. Finally, while CNN has a strong structure, INR-based approaches have shown tremendous potential for both 3D and 2D tasks.

2.2 Implicit Neural Representation

Recently, implicit representations of 3D objects, scenes and shapes have gained significant momentum in research. Traditional discrete explicit representations have been partly replaced by implicit neural representations (INR), which use parameterized MLPs to map coordinate information into signals (coor-MLP) in the target domain. For example, NeRF [18] expanded the input 3D coordinate to a continuous 5D scene representation with a 2D viewing direction, resulting in better renderings of high-frequency scene content than explicit 3D representations such as voxel methods, point cloud, and mesh. DeepSDF [20] takes a 3D coordinate and a categorical latent code as input and outputs the signed distance (SDF) at this

coordinate to determine whether it is inside the target shape. Related works have enhanced INR's ability to model 3D surfaces and shapes [1, 12, 17, 26]. This approach has also been extended to the 2D domain, for example, Local Implicit Image Function (LIIF) [2] extracts a set of latent codes distributed in the LR domain to interpolate the HR target image. Based on LIIF, UltraSR [36] attempts to apply residual structure to the 2D INR process and add the multiple injection of coordinate information and residual structure. Furthermore, LTE [14] proposes a local texture estimator to characterize the image information into the Fourier domain and incorporate it with the coordinate information as input to the MLP. SIREN [25] proposes an overall implicit neural representation framework to adapt the complex natural signals and their derivatives using a periodic activation function. CRM [23] performs image segmentation refinement using implicit neural representations. When applied to processing multimodal data, JIIF [28] proposes using INR to reconstruct depth images in the HR domain by using LR domain RGB images guided with noisy low-resolution depth images. This work strongly inspired us to use INR to process multispectral and hyperspectral Image Fusion. However, previous work has demonstrated the limitations and biases of the MLP-ReLU structure in learning high-frequency information [21]. Therefore, we focus on designing strategies for the fusion process of different modes to improve the performance of high-frequency representation and add a decoder after the MLP layer to correct the bias.

2.3 Motivation

LR-HSI and HR-MSI provide abundant spectral and spatial information, respectively, making them a valuable resource for image analysis. However, fully utilizing the local content of these images and fusing information from different modalities, such as spatial, spectral, and coordinate, are challenging. To address this issue, we propose an implicit neural fusion network (INFN) that relies on the implicit neural representation (INR) of the image. The INR-based approaches have demonstrated exceptional performance in arbitrary-scaled image super-resolution tasks [2], frequently employing a multilayer perceptron (MLP) as the fusion component. However, MLPs tend to acquire low-frequency information, necessitating additional input of high-frequency data, such as position or frequency encoding [27, 36]. To overcome this limitation, we introduce the implicit neural feature fusion function (INF³). Inspired by the multiscale injection branch of SSconv [33], in INF³ we inject detailed high-frequency information in dual scales, specifically using MLPs to learn high-frequency data for MHIF task. Additionally, we address the challenge of identifying feature vectors that are close in distance but different in angle by proposing that our INF³ utilizes cosine similarity between feature vectors to compute coefficients. In detail, we utilize full-size and reduced-size HR-MSI to generate interpolated weights, eliminating the need for network learning or additional parameters. As a result, our fusion framework has demonstrated state-of-the-art performance on two publicly available datasets.

3 METHODOLOGY

In this section, we present our INF³ representation designed for the MHIF task. We first introduce the overall architecture of our

implicit neural fusion network (INFN) in Sec. 3.1. Subsequently, we review recent implicit neural representations (INR) for 2D tasks in Sec. 3.2. Finally, we describe the design of INF³ in Sec. 3.3 for the fusion process.

3.1 The Overall Architecture

As shown in Fig. 2, the INFN is generally divided into two segments: encoder and decoder. In practice, it is evident that directly applying an INR-based approach to address MHIF tasks often leads to overfitting. To overcome this challenge and ensure network stability during training, we have opted for an encoder-decoder architecture. Supplementary materials will include relevant ablation experiments. Specifically, the encoder stage can be formulated as follows:

$$\mathcal{E} = \text{Encoder}(\mathcal{X}, \mathcal{Y}, C), \quad (1)$$

where $\mathcal{E} \in \mathbb{R}^{H \times W \times D}$ represents the fusion result of the encoder, $\mathcal{X} \in \mathbb{R}^{h \times w \times S}$ denotes the LR-HSI, $\mathcal{Y} \in \mathbb{R}^{H \times W \times s}$ denotes the HR-MSI, and $C \in \mathbb{R}^{H \times W \times 2}$ is the normalized 2D coordinate map in the high resolution (HR) domain. In detail, we propose to represent a pixel by its center position and scale the coordinate map of $H \times W$ into the square grid of size $[-1, 1] \times [-1, 1]$ to make it convenient to share the coordinates in both the HR and LR domains. The normalization process in HR domain can be formulated as:

$$C(i, j) = \left[-1 + \frac{2i+1}{H}, -1 + \frac{2j+1}{W} \right], \quad (2)$$

where $i \in [0, H-1]$, $j \in [0, W-1]$. To deal with information about different modes, *i.e.*, LR-HSI and HR-MSI, we utilize function F_ψ and function F_ϕ to extract the spatial and spectral information, respectively. The process of spectral function can be formulated as follows:

$$\mathcal{S}_{pe} = F_\phi(\mathcal{X}), \quad (3)$$

where $\mathcal{S}_{pe} \in \mathbb{R}^{h \times w \times D_1}$ is the feature map of spectral modality and ϕ is learnable parameters of spectral function. D_1 is the number of output channels of the spectral function. To extract information from spatial modality, we propose to concatenate bicubic interpolated LR-HSI $\mathcal{X}^U \in \mathbb{R}^{H \times W \times S}$ with the HR-MSI $\mathcal{Y} \in \mathbb{R}^{H \times W \times s}$, thus inputting it into the spatial function f_ψ for extracting. In special, this process can be expressed by the formula:

$$\mathcal{S}_{pa} = F_\psi(\text{Cat}(\mathcal{X}^U, \mathcal{Y})), \quad (4)$$

where $\mathcal{S}_{pa} \in \mathbb{R}^{H \times W \times D_2}$ is the feature map of spatial modality and ψ is learnable parameters of spatial function. D_2 is the number of output channels of the spatial function. In addition, $\text{Cat}(\cdot)$ means the concatenation operation in channel dimension. We view the INF³ framework as the key of encoder, which can be formulated as:

$$\mathcal{E} = \text{INF}^3(\mathcal{S}_{pe}, \mathcal{S}_{pa}, C). \quad (5)$$

For the decoding process, we work on the encoding output $\mathcal{E} \in \mathbb{R}^{H \times W \times C}$ to generate the decoding result $\mathcal{D} \in \mathbb{R}^{H \times W \times S}$ via a two-layer convolution structure. The parameters of the decoder are shared by all training patches. In general, the neural network tends to predict frequencies located near a low frequency region. Yet, past work has proved that a long skip connection in local implicit representation enriches high-frequency components in residuals and stabilizes convergence [13]. Thus, we add the bicubic

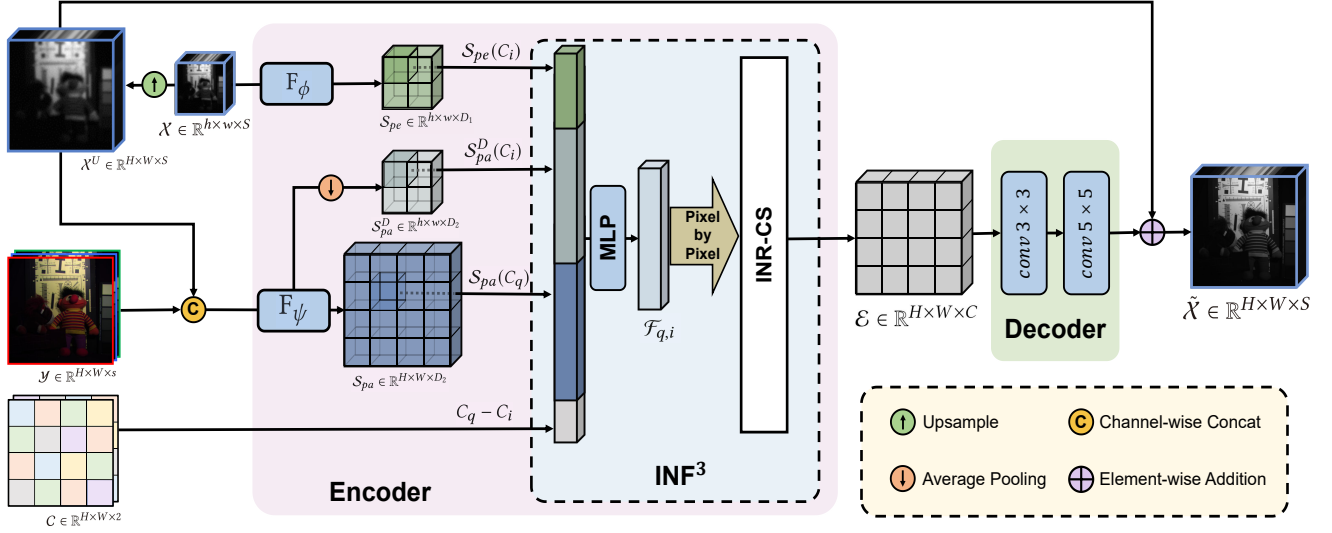


Figure 2: The overall architecture of the proposed INFN, which consisted of two segments: encoder and decoder. Specifically, we input three modal information such as LR-HSI X , HR-HSI Y and coordinate C into the encoder, and subsequently put the encoded result into the decoder and add it with up-sampled LR-HSI X^U to get the final output \hat{X} . The INR-CS is described with detail in Sec. 3.2 and Sec. 3.3.

interpolation LR-HSI X^U as a long skip connection to ameliorate the above problem. Thus, the final signal take the form:

$$\hat{X} = \text{Decoder}(\mathcal{E}) + X^U. \quad (6)$$

3.2 Implicit Neural Representation

In this session, we will introduce the implicit neural representation (INR) from the perspective of interpolation method. Given a low-resolution image $x \in \mathbb{R}^{h \times w \times 3}$ and the corresponding high-resolution (HR) interpolated image $\hat{x} \in \mathbb{R}^{H \times W \times 3}$ as an example, the INR up-sampling process at position C_q can be expressed as:

$$\hat{x}(C_q) = \sum_{i \in \mathcal{N}_q} w_{q,i} v_{q,i}, \quad (7)$$

where $C_q \in \mathbb{R}^2$ is the normalized coordinate of the query pixel in the HR domain, $\mathcal{N}_q \in \mathbb{R}^4$ is the coordinate of neighbor pixels for C_q in the LR domain, $w_{q,i} \in \mathbb{R}$ is the interpolation weight of $v_{q,i} \in \mathbb{R}^{1 \times 1 \times 3}$, and $v_{q,i}$ is the vector of x . The interpolation weights are usually normalized so that $\sum_{i \in \mathcal{N}_q} w_{q,i} = 1$. Previous work usually proposes to set \mathcal{N}_q to the pixels at the four nearest centers of C_q in the LR domain. The calculation of the interpolation weights varies from articles to articles, and the simplest formulation of area weight interpolation used by LIIF [2] is as follows:

$$w_{q,i} = \frac{A_i}{A}, \quad (8)$$

where A_i is the partial area diagonally opposite to the i corner pixel, $A = \sum_{i \in \mathcal{N}_q} A_i$ is the total area serving as the denominator. In detail, the LIIF fuses LR pixel information with HR relative coordinate information through MLP to generate the interpolation value $v_{q,i}$, which takes the following form:

$$v_{q,i} = \text{MLP}_\Theta(x(C_i), C_q - C_i), \quad (9)$$

where $\text{MLP}_\Theta(\cdot)$ is an MLP layer with learnable parameters Θ that takes a local feature vector $x(C_q)$ in the LR domain and a relative coordinate $C_q - C_i$ as inputs. From the above equations, the interpolated vector can be represented by a set of local feature vectors in the LR domain, which stores the low-resolution information of the local region. In general, INR-based methods implement up-sampling by querying $x(C_q)$ with the relative query coordinate $C_q - C_i$ in the arbitrary super-resolution task.

3.3 Implicit Neural Feature Fusion Function

The objective of the MHIF task is to fuse the different modal inputs of LR-HSI and HR-MSI, resulting in the generation of HR-HSI with high spectral and spatial resolution. Previous fusion techniques usually construct two separate CNN branches for the LR-HSI and HR-MSI [38], and then extract sets of CNN features [6, 11, 16]. However, the CNN-based fusion methods are significantly dependent on stacking convolution structures and lack interpretability. Inspired by the recent developments in INR [2, 28], we propose a multimodal and multiscale fusion function based on the INR framework, and use parameter-free weight generation method to facilitate the mining of high-frequency information in the fusion process. In summary, we innovatively create the Implicit Neural Feature Fusion Function (INF³) to guide the fusion process. Unlike the LIIF [2] representation, which directly generates the predicted signal, our INF³ is designed to generate the fused feature map $\mathcal{E} \in \mathbb{R}^{H \times W \times C}$, and then use a decoder structure to work out our final output \hat{X} . Specifically, the fused feature map \mathcal{E} at position C_q can be represented as follows:

$$\mathcal{E}_q = \sum_{i \in \mathcal{N}_q} w_{q,i} \mathcal{F}_{q,i}, \quad (10)$$

where \mathcal{N}_q indicates the set of the four nearest query coordinates around C_q in the normalized HR domain, $w_{q,i}$ and $\mathcal{F}_{q,i}$ are the

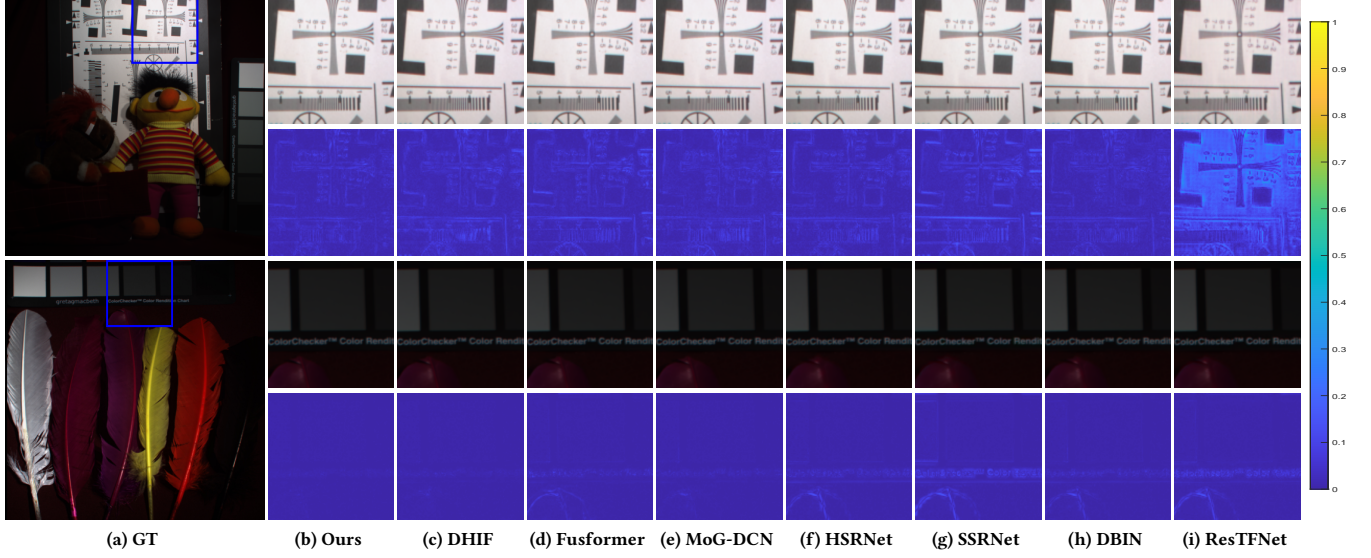


Figure 3: The first and third rows show the results using the pseudo-color representation on “chart and stuffed toy” and “feathers”, respectively, from the CAVE dataset. Some close-ups are depicted in the blue rectangles. The second and fourth rows show the residuals between the GT and the fused products. (a) GT, (b) Ours, (c) DHIF [11], (d) Fusformer [9], (e) MoG-DCN [6], (f) HSRNet [10], (g) SSRNet [38], (h) DBIN [32] and (i) ResTFNet [16].

weights and multimodal fusion information of query coordinate C_q at position C_i , respectively. Typically, we regard $\mathcal{F}_{q,i} \in \mathbb{R}^{1 \times 1 \times C}$ as the fused feature vector at position C_i when querying coordinate C_q . In the following passage, we will introduce how to generate $\mathcal{F}_{q,i}$ and $w_{q,i}$.

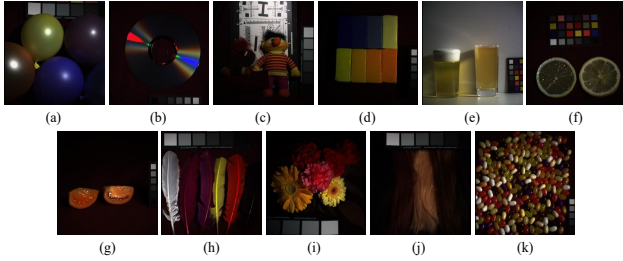


Figure 4: The testing images from the CAVE dataset: (a) balloons, (b) cd, (c) chart and stuffed toy, (d) clay, (e) fake and real lemons, (f) fake and real tomatoes, (g) fake and real lemons, (h) feathers, (i) flowers, (j) hairs, and (k) jelly beans. An RGB color representation is used to depict the images.

Dual high-frequency fusion: We observe that different resolution information plays an important role in MHIF tasks. To this end, we design a structure, i.e., dual high-frequency fusion (DHFF), which combines high-frequency spatial information at different resolutions. Firstly, we concatenate the LR domain spatial information $S_{pa}^D \in \mathbb{R}^{h \times w \times D_2}$ and spectral information $S_{pe} \in \mathbb{R}^{h \times w \times D_1}$ vectors at position C_i , which can be formulated as follows:

$$\mathcal{F}_{q,i}^1 = \text{Concat}(S_{pe}(C_i), S_{pa}^D(C_i)), \quad (11)$$

where $\mathcal{F}_{q,i}^1 \in \mathbb{R}^{1 \times 1 \times (D_1 + D_2)}$ is the fusion of spectral information and spatial information at the same resolution. Specifically, we

generate LR domain high-frequency spatial information, i.e., S_{pa}^D by the following formula:

$$S_{pa}^D = \text{Mean}(S_{pa}). \quad (12)$$

Given the up-sampling ratio is r , we operate mean operation on the $r \times r$ region of $S_{pa} \in \mathbb{R}^{H \times W \times D_2}$ and then get the $S_{pa}^D \in \mathbb{R}^{h \times w \times D_2}$. This design is to incorporate the LR domain high-frequency information, to better serve the MLP layer. In Sec. 4.1, we will design relevant ablation study and verify the effectiveness of this design. Secondly, we combine HR domain information $S_{pa} \in \mathbb{R}^{H \times W \times D_2}$ at position C_q with LR domain fusion information $\mathcal{F}_{q,i}^1$. The process above can be expressed as:

$$\mathcal{F}_{q,i}^2 = \text{Concat}(\mathcal{F}_{q,i}^1, S_{pa}(C_q)), \quad (13)$$

where $\mathcal{F}_{q,i}^2 \in \mathbb{R}^{1 \times 1 \times (D_1 + D_2 + D_2)}$ serves as the result of DHFF. In general, our DHFF naturally combines feature vectors of different modalities and different scales with the aim of making the MLP acquire both spatial and spectral information. Similar to the previous INR-based work, we obtain the coordinate modal information by adding the relative positions of C_q and C_i to the fusion process, which can be represented as:

$$\mathcal{F}_{q,i}^3 = \text{Concat}(\mathcal{F}_{q,i}^2, C_q - C_i), \quad (14)$$

where $\mathcal{F}_{q,i}^3 \in \mathbb{R}^{1 \times 1 \times (D_1 + D_2 + D_2 + 2)}$ is the result after adding the relative distance information of interpolation on the basis of $\mathcal{F}_{q,i}^2$. Finally, we utilize an MLP layer to learn the information in $\mathcal{F}_{q,i}^3$ and get the following expression:

$$\mathcal{F}_{q,i} = \text{MLP}_{\Theta}(\mathcal{F}_{q,i}^3), \quad (15)$$

where $\mathcal{F}_{q,i} \in \mathbb{R}^{1 \times 1 \times C}$ is multimodal fusion information of query coordinate C_i when querying coordinate C_q . $\text{MLP}_\Theta(\cdot)$ is a fully connected layer, and Θ serves as its learnable parameters.

Cosine similarity: The proposed INR with cosine similarity (INR-CS) method generates weights based on cosine similarity. In Eq. (10), $w_{q,i} \in \mathbb{R}$ is the weight at the position C_i when querying the coordinate C_i . Part of the previous work viewed the generation of this weight simply as a solution to the interpolation problem, using area-based method to generate the target weights [2], which ignores local texture and information about the data itself. The other part of the work proposes to learn the weights by network parameters, *i.e.*, learning similar weights by graph attention mechanisms [28] which lacks of interpretability. In order to utilize information about $\mathcal{F}_{q,i}$ while keeping interpretability, we propose a parameter-free approach named INR-CS as follows:

$$w_{q,i} = \frac{\exp(\|\mathcal{F}_{q,\hat{q}}^1\| \cdot \|\mathcal{F}_{q,i}^1\| \langle \mathcal{F}_{q,\hat{q}}^1, \mathcal{F}_{q,i}^1 \rangle)}{w_q}, \quad (16)$$

where

$$w_q = \sum_{i \in \mathcal{N}_q} \exp(\|\mathcal{F}_{q,\hat{q}}^1\| \cdot \|\mathcal{F}_{q,i}^1\| \langle \mathcal{F}_{q,\hat{q}}^1, \mathcal{F}_{q,i}^1 \rangle). \quad (17)$$

$\mathcal{F}_{q,i}^1$ is given by Eq. (11), where the \hat{q} is the closest point to C_q in the LR domain. In detail, $\mathcal{F}_{q,\hat{q}}^1 = \text{Concat}(\mathcal{S}_{pa}^D(\hat{q}), \mathcal{S}_{pe}(\hat{q}))$, and $\langle \cdot, \cdot \rangle$ represents the cosine operation between vectors. The similarity between feature vectors is normalized by the softmax function.

4 EXPERIMENT

Datasets: Following the previous studies, we conduct experiments to evaluate our model on the CAVE¹ and Harvard² datasets. In detail, the CAVE dataset contains 32 HSIs with 31 spectral bands ranging in wavelengths from 400 nm to 700 nm in increments of 10 nm. We randomly select 20 images for training, and the remaining 11 images make up the testing dataset. In addition, the Harvard dataset includes 77 HSIs of both indoor and outdoor scenes, with each HSI having a size of $1392 \times 1040 \times 31$ and spanning the 420 nm to 720 nm spectral range. We chose 20 of them and crop the upper left portion (1000×1000), with the 10 images being utilized for testing and the remaining 10 were used for training.

Data Simulation: We input LR-HSI and HR-MSI $(\mathcal{X}, \mathcal{Y})$ pairs into the end-to-end network, and use HR-HSI $\tilde{\mathcal{X}}$ for training. Due to ground-truth (GT) $\tilde{\mathcal{X}}$ is not available in real life, a simulation process is thus required. As for CAVE dataset, we crop the 20 selected training images to generate 3920 overlapping patches with the dimension $64 \times 64 \times 31$, and this patches will serve as GT $\tilde{\mathcal{X}}$. In order to generate the proper LR-HSIs, we use a 3×3 Gaussian kernel with a standard deviation of 0.5 to blur the initial HR-HSIs and downsample the blurred patches with a scaling factor of 4. Additionally, we utilize the common spectral response function of the Nikon D700³ camera and HR-HSIs to create the HR-MSI patches. Thus, we generate 3920 LR-HSIs with a size of $16 \times 16 \times 31$ and HR-MSIs with a size of $64 \times 64 \times 3$ form the input pairs $(\mathcal{X}, \mathcal{Y})$. Following that, the inputs pairs and associated GTs are divided at random into training data (80%) and testing data (20%). To create

the input LR-HSI and HR-MSI products as well as the GTs, this method is also applied to the Harvard dataset.

Benchmark: To verify the superiority of the proposed INF³, we compare it with various state-of-the-art methods including MTF-GLP-HS [22], CSTF-FUS [15], LTTR[4], LTMR[3], IR-TenSR[35], DBIN [32], SSRNet [38], ResTFNet [16], HSRNet [10], MoG-DCN [6], Fusformer [9] and the DHIF [11] network. In specific, the upsampled LR-HSI in Fig. 2 is the bicubic-interpolated result, which is added to the experiment as a baseline. By the way, all the deep learning approaches are trained with the same input pairs for a fair comparison. Moreover, the related hyperparameters are selected consistent with the original papers.

Implementation Details: The proposed network implements in PyTorch 1.11.0 and Python 3.8.0 using Adam optimizer[19] with a learning rate of 0.0001 to minimize sum of absolute difference \mathcal{L}_1 by 1000 epochs and Linux operating system with a NVIDIA RTX3080 GPU (12GB).

Results on CAVE Dataset: In this section, we evaluate the effectiveness of our proposed INF³ method on the CAVE dataset (scaling factor of 4) and compare it with existing MHIF methods. As shown in the left part of Tab. 1, our INF³ outperforms other state-of-the-art deep learning models by a large margin. For instance, our INF³ improves PSNR by 1.31 dB, 2.40 dB, 0.75 dB, and 2.00 dB compared with DHIF [11], Fusformer [9], MoG-DCN [6], and HSRNet [10], respectively. The proposed INF³ achieves significant improvements in two QIs, *i.e.*, SAM and ERGAS. In particular, our INF³ improves ERGAS by 11.71% and 18.33%, compared with the second and third best models. In addition, our INF³ outperforms MoG-DCN [6] and DHIF [11] on SAM and has only two-fifths and one-seventh of their parameters. Moreover, to aid in visual verification, we provide pseudo-color depictions of the fused products and some error maps in Fig.3. It can be observed that the generated results of our INF³ are very close to the ground truth and maintain better reconstruction quality with more accurate textures. Regarding the absolute error maps in Fig.3, the closer the reconstruction impact is to the original picture, the more blue the error map's color is. It is evident that INF³ restores texture details better than the other techniques under comparison, which is consistent with the analysis in Tab. 1.

Results on Harvard Dataset: Fig.6 displays 10 test images from the Harvard dataset. Moreover, the right-hand portion of Tab.1 presents the comparison results of five indices obtained by all compared methods on another hyperspectral image dataset, namely Harvard, for a scaling factor of 4. It is evident that the average PSNR value of our proposed INF³ is higher by 0.17 dB and 0.51 dB compared to the second-best and third-best methods, respectively. Although our model is slightly inferior to the second-best MoG-DCN [6] in terms of SAM, our model's parameters are only two-fifths of MoG-DCN's. Moreover, our model achieves the best results on ERGAS and SSIM, indicating the best structural recovery. Furthermore, Fig. 5 illustrates that our proposed INF³ is capable of reconstructing the detailed structure of the original image. Notably, our method restores the finest details of the bike, the metallic sheen, and the texture of the backpack. These error maps also demonstrate that our proposed INF³ achieves the best fidelity in terms of texture details. Additionally, the fact that our residuals are closer to blue indicates that our recovery is better than other methods.

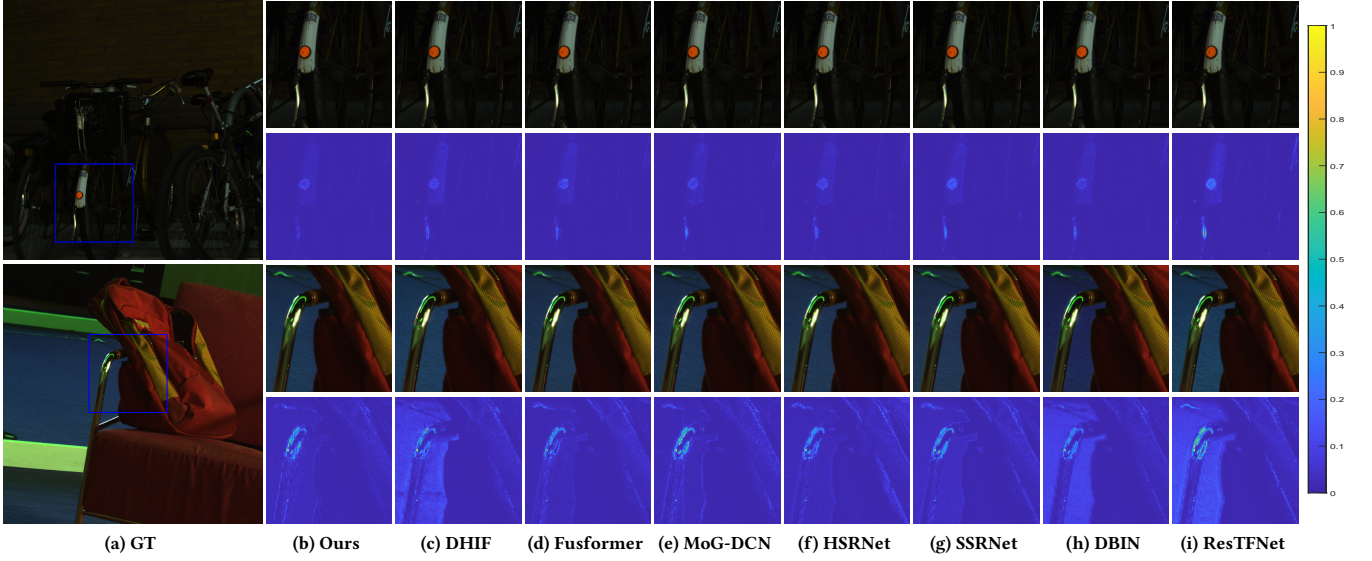
¹<https://www.cs.columbia.edu/CAVE/databases/multispectral/>

²<http://vision.seas.harvard.edu/hyperspec/index.html>

³http://www.maxmax.com/nikon_d700_study.htm

Table 1: Average quantitative comparisons on 11 CAVE examples and 10 Harvard examples simulating a scaling factor of 4. The best values are highlighted in red, and the second best values are signed in blue. M refers to millions.

Methods	CAVE					Harvard				
	PSNR	SAM	ERGAS	SSIM	#params	PSNR	SAM	ERGAS	SSIM	#params
Bicubic	34.33±3.88	4.45±1.62	7.21±4.90	0.944±0.0291	—	38.71±4.33	2.53±0.67	4.45±41.81	0.948±0.0268	—
MTF-GLP-HS [22]	37.69±3.85	5.33±1.91	4.57±2.66	0.973±0.0158	—	33.81±3.50	6.25±2.42	3.47±1.82	0.952±0.0321	—
CSTF-FUS [15]	34.46±4.28	14.37±5.30	8.29±5.29	0.866±0.0747	—	39.13±3.50	6.91±2.66	4.64±1.80	0.913±0.0487	—
LTTR [4]	35.85±3.49	6.99±2.55	5.99±2.92	0.956±0.0288	—	37.91±3.58	5.35±1.94	2.44±1.06	0.972±0.0183	—
LTMR [3]	36.54±3.30	6.71±2.19	5.39±2.53	0.963±0.0208	—	38.41±3.58	5.05±1.70	2.24±0.97	0.970±0.0166	—
IR-TenSR [35]	35.61±3.45	12.30±4.68	5.90±3.05	0.945±0.0267	—	40.47±3.04	4.36±1.52	5.57±1.57	0.962±0.0140	—
DBIN [32]	50.83±4.29	2.21±0.63	1.24±1.06	0.996±0.0026	0.469M	47.88±3.87	2.31±0.46	1.95±0.81	0.988±0.0066	0.469M
ResTFNet [16]	45.58±5.47	2.82±0.70	2.36±2.59	0.993±0.0056	2.387M	45.93±4.35	2.61±0.69	2.56±1.32	0.985±0.0082	2.387M
SSRNet [38]	48.62±3.92	2.54±0.84	1.63±1.21	0.995±0.0023	0.027M	47.95±3.37	2.31±0.60	2.30±1.42	0.987±0.0070	0.027M
HSRNet [10]	50.38±3.38	2.23±0.66	1.20±0.75	0.996±0.0014	0.633M	48.29±3.03	2.26±0.56	1.87±0.81	0.988±0.0064	0.633M
MoG-DCN [6]	51.63±4.10	2.03±0.62	1.11±0.82	0.997±0.0018	6.840M	47.89±4.09	2.11±0.52	1.89±0.82	0.988±0.0073	6.840M
Fusformer [9]	49.98±8.10	2.20±0.85	2.50±5.21	0.994±0.0111	0.504M	47.87±5.13	2.84±2.07	2.04±0.99	0.986±0.0101	0.467M
DHIF [11]	51.07±4.17	2.01±0.63	1.22±0.97	0.997±0.0016	22.462M	47.68±3.85	2.32±0.53	1.95±0.92	0.988±0.0074	22.462M
INF ³ (ours)	52.36±3.93	1.99±0.60	0.99±0.73	0.997±0.0013	2.902 M	48.46±3.43	2.14±0.52	1.83±0.76	0.989±0.0064	2.902 M
Ideal value	∞	0	0	1	-	∞	0	0	1	-

**Figure 5:** The first and third rows show the results using the pseudo-color representation from the Harvard dataset. Noting that we select three bands (31-20-10) from HSIs as the red, green and blue channels. We zoomed in on the blue rectangles to show more detail. The second and fourth rows show the residuals between the GT and the fused products. (a) GT, (b) Ours, (c) DHIF [11], (d) Fusformer [9], (e) MoG-DCN [6], (f) HSRNet [10], (g) SSRNet [38], (h) DBIN [32] and (i) ResTFNet [16].

4.1 Ablation Study

In this section, we profoundly discuss the effectiveness of dual high-frequency fusion (DHIF), which combines LR and HR domain in the INF³. Our primary concern is whether injecting relative location information can aid the network in image recovery. Therefore, we conducted an ablation study to assess this. Furthermore, we included the proposed weight generation method in the ablation

study. To maintain brevity and generality, the analysis is conducted on the CAVE dataset.

1) *Dual high-frequency fusion*: To evaluate the effectiveness of dual-high-frequency information injection, we conducted several experiments. As shown in Tab. 2, we found that the removal of high-frequency information injection in HR domain resulted in a significant decline in the performance of INF³. This indicates that high-resolution and high-frequency information provides more

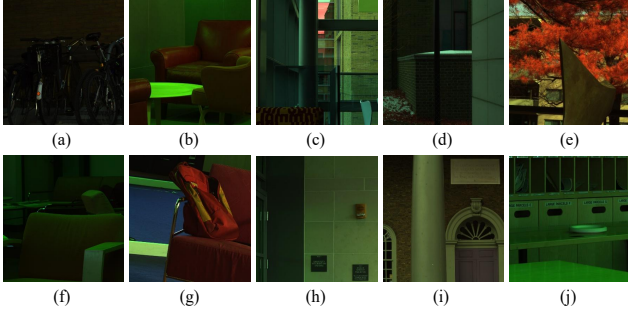


Figure 6: The 10 images tested on the Harvard dataset are (a) bikes, (b) sofa1, (c) window, (d) fence, (e) tree, (f) sofa2, (g) backpack, (h) wall, (i) door and (j) parcels.

Table 2: The average four QIs and the corresponding parameters on the CAVE dataset simulating a scaling factor of 4. LR and HR mean low-resolution and high-resolution domain high-frequency information injection, respectively.

LR	HR	PSNR	SAM	ERGAS	SSIM
✓	✗	42.55±2.58	2.91±0.93	2.82±1.74	0.990±0.0020
✗	✓	52.17±4.02	2.01±0.61	1.02±0.77	0.997±0.0014
✓	✓	52.36±3.93	1.99±0.60	0.99±0.73	0.997±0.0013

detailed information during the fusion process of INF³. Moreover, the performance of INF³ slightly decreased when LR domain high-frequency information injection was removed, suggesting that high-frequency information of LR domain plays a supportive role in the fusion process. The utilization of different resolution information resulted in the best performance for our INF³. The importance of information at various resolutions for MHIF tasks inspired us to design this structure, and the experiments supported the rationality behind this design.

Table 3: The average four QIs and the corresponding parameters on the CAVE dataset simulating a scaling factor of 4. δ_c means the relative coordinate $C_q - C_i$.

δ_c	PSNR	SAM	ERGAS	SSIM
✗	52.22±3.92	1.98±0.58	1.00±0.74	0.997±0.0013
✓	52.36±3.93	1.99±0.60	0.99±0.73	0.997±0.0013

2) *Relative coordinate* : In this section, we will analyze the effectiveness of the relative coordinate $C_q - C_i$ in INF³. The relative coordinate and pixels belong to different modalities, where the former represents the distance of interpolation, and the latter represents the value of interpolated value. We are curious whether the information from different modalities can aid the MLP in understanding the fusion and interpolation processes in INF³. To address this, we conducted an ablation experiment to eliminate our confusion. Specifically, we removed the relative coordinate from INF³ while keeping the rest unchanged. Tab. 3 presents our results, showing that the inclusion of the relative coordinate improves the network’s understanding of the MHIF task and has a positive impact on its realization.

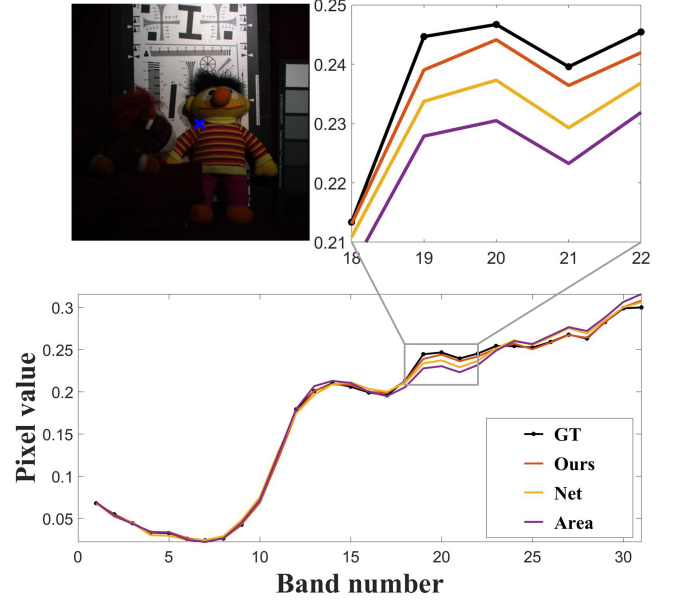


Figure 7: The blue cross on the top left image ‘chart and stuffed toy’ shows where the spectral vector is located, while the top right picture and the bottom picture represent the spectral vector at position (276, 260). The bottom picture displays the output of the network-based and area-based weight generation methods, denoted by ‘Net’ and ‘Area’, respectively. Table 4: The four QIs and the corresponding parameters on the image ‘balloons’ simulating a scaling factor of 4. Net-based and Area-based represent the method of generating weights based on network and area in JIIF [28] and LIIF [2], respectively.

Methods	PSNR	SAM	ERGAS	SSIM
Area-based	54.741	1.294	0.335	0.9978
Net-based	54.392	1.281	0.350	0.9977
Ours	54.813	1.283	0.331	0.9978

3) *Weight generation method*: To assess the superiority of our cosine similarity method, we conducted a comparison with area-based and network-based weight generation methods on the CAVE dataset, with INF³ serving as the backbone. As shown in Tab. 4, our approach significantly outperforms the other methods on certain images, such as ‘chart and stuffed toy’. To further illustrate the possible spectral distortions in the fused products, we visualized the spectral vectors. Fig.7 shows the spectral vectors for the 31 bands at position (276, 260) in the ‘chart and stuffed toy’ image. For the purpose of clarity, we have zoomed in on the spectral vectors of the 18th-22th bands, as indicated by the rectangular boxes in Fig.7. In both the figures, it is evident that the spectral vectors of the proposed method (the red lines) are the closest to the ground truth (GT).

4) *Upsampling methods*: In this section, we present experiments that compare INF³ with other upsampling methods. Intuitively, INF³ can be regarded as an interpolation algorithm. Unlike traditional interpolation algorithms, it provides each interpolated point with

Table 5: The average four QIs and the corresponding parameters on the CAVE dataset simulating a scaling factor of 4. M means a million.

Methods	PSNR	SAM	ERGAS	SSIM	#params
Bilinear	51.93±3.99	2.05±0.62	1.04±0.78	0.997±0.0017	3.003 M
Bicubic	51.98±4.06	2.04±0.61	1.04±0.79	0.997±0.0018	3.003 M
Pixel shuffle	52.15±4.27	1.98±0.58	1.04±0.83	0.997±0.0020	7.722 M
Ours	52.36±3.93	1.99±0.60	0.99±0.73	0.997±0.0013	2.902 M

additional relative position information via the MLP layer, which incorporates multi-modal information. Specifically, we compared INF³ with pixel-shuffle [24] and traditional interpolation methods that are commonly used in convolutional neural networks. As shown in Tab. 5, our INF³ outperforms other methods in terms of MHIF tasks with fewer parameters.

5 CONCLUSION

In this paper, we propose the Implicit Neural Feature Fusion Function (INF³) and design an Implicit Neural Fusion Network (INFN) based on it for multispectral and hyperspectral image fusion task. Unlike previous CNN-based approaches, we novelly fuse multi-modal information including coordinate, spatial and spectral data for multiple times, and accordingly modify the previous Implicit Neural Representation of upsampling interpolation to make better use of high-frequency information. By training two different branches of the encoder, the input information is fused in two stages and entered within the INR framework, whose effectiveness in utilizing high-frequency information has also been verified. The INF³-based process also provides a generalized paradigm for other multimodal fusion tasks. Experimental results demonstrate that our method can achieve state-of-the-art performance on two different datasets. Moving forward, we will persist in exploring dependable network-based interpolation fusion methods and stable weight generation techniques.

REFERENCES

- [1] Rohan Chabra, Jan E Lenssen, Eddy Ilg, Tanner Schmidt, Julian Straub, Steven Lovegrove, and Richard Newcombe. 2020. Deep local shapes: Learning local sdf priors for detailed 3d reconstruction. In *Computer Vision—ECCV 2020: 16th European Conference, Glasgow, UK, August 23–28, 2020, Proceedings, Part XXIX* 16. Springer, 608–625.
- [2] Yinbo Chen, Sifei Liu, and Xiaolong Wang. 2021. Learning continuous image representation with local implicit image function. In *Proceedings of the IEEE/CVF conference on computer vision and pattern recognition*. 8628–8638.
- [3] Renwei Dian and Shutao Li. 2019. Hyperspectral image super-resolution via subspace-based low tensor multi-rank regularization. *IEEE Trans. Image Process.* 28, 10 (2019), 5135–5146.
- [4] Renwei Dian, Shutao Li, and Leyuan Fang. 2019. Learning a low tensor-train rank representation for hyperspectral image super-resolution. *IEEE Trans. Neural Netw. Learn. Syst.* 30, 9 (2019), 2672–2683.
- [5] Weisheng Dong, Peiyao Wang, Wotao Yin, Guangming Shi, Fangfang Wu, and Xiaotong Lu. 2018. Denoising prior driven deep neural network for image restoration. *IEEE transactions on pattern analysis and machine intelligence* 41, 10 (2018), 2305–2318.
- [6] Weisheng Dong, Chen Zhou, Fangfang Wu, Jinjian Wu, Guangming Shi, and Xin Li. 2021. Model-guided deep hyperspectral image super-resolution. *IEEE Trans. Image Process.* 30 (2021), 5754–5768.
- [7] Mathieu Fauvel, Yuliya Tarabalka, Jon Atli Benediktsson, Jocelyn Chanussot, and James C Tilton. 2012. Advances in spectral-spatial classification of hyperspectral images. *Proc. IEEE* 101, 3 (2012), 652–675.
- [8] Kaiming He, Xiangyu Zhang, Shaoqing Ren, and Jian Sun. 2016. Deep residual learning for image recognition. In *Proceedings of the IEEE conference on computer vision and pattern recognition*. 770–778.
- [9] Jinfan Hu, Tingzhu Huang, Liangjian Deng, Hongxia Dou, Danfeng Hong, and Gemine Vivone. 2022. Fusformer: A Transformer-Based Fusion Network for Hyperspectral Image Super-Resolution. *IEEE Geosci. Remote Sens. Lett.* 19 (2022), 1–5.
- [10] Jinfan Hu, Tingzhu Huang, Liangjian Deng, Taixiang Jiang, Gemine Vivone, and Jocelyn Chanussot. 2021. Hyperspectral image super-resolution via deep spatio-spectral attention convolutional neural networks. *IEEE Trans. Neural Netw. Learn. Syst.* (2021).
- [11] Tao Huang, Weisheng Dong, Jinjian Wu, Leida Li, Xin Li, and Guangming Shi. 2022. Deep Hyperspectral Image Fusion Network With Iterative Spatio-Spectral Regularization. *IEEE Trans. Comput. Imaging*, 8 (2022), 201–214.
- [12] Chiyu Jiang, Avneesh Sud, Ameesh Makadia, Jingwei Huang, Matthias Nießner, Thomas Funkhouser, et al. 2020. Local implicit grid representations for 3d scenes. In *Proceedings of the IEEE/CVF Conference on Computer Vision and Pattern Recognition*. 6001–6010.
- [13] Jiwon Kim, Jung Kwon Lee, and Kyoung Mu Lee. 2016. Accurate image super-resolution using very deep convolutional networks. In *Proceedings of the IEEE conference on computer vision and pattern recognition*. 1646–1654.
- [14] Jaewon Lee and Kyong Hwan Jin. 2022. Local texture estimator for implicit representation function. In *Proceedings of the IEEE/CVF Conference on Computer Vision and Pattern Recognition*. 1929–1938.
- [15] Shutao Li, Renwei Dian, Leyuan Fang, and José M Bioucas-Dias. 2018. Fusing hyperspectral and multispectral images via coupled sparse tensor factorization. *IEEE Trans. Image Process.* 27, 8 (2018), 4118–4130.
- [16] Xiangyu Liu, Qingjie Liu, and Yunhong Wang. 2020. Remote sensing image fusion based on two-stream fusion network. *Inf. Fusion*, 55 (2020), 1–15.
- [17] Mateusz Michalkiewicz, Jhony K Pontes, Dominic Jack, Mahsa Baktashmotlagh, and Anders Eriksson. 2019. Implicit surface representations as layers in neural networks. In *Proceedings of the IEEE/CVF International Conference on Computer Vision*. 4743–4752.
- [18] Ben Mildenhall, Pratul P Srinivasan, Matthew Tancik, Jonathan T Barron, Ravi Ramamoorthi, and Ren Ng. 2021. Nerf: Representing scenes as neural radiance fields for view synthesis. *Commun. ACM* 65, 1 (2021), 99–106.
- [19] Kingma Diederik P and Jimmy Ba. 2014. Adam: A method for stochastic optimization. *International Conference on Learning Representations* (2014).
- [20] Jeong Joon Park, Peter Florence, Julian Straub, Richard Newcombe, and Steven Lovegrove. 2019. DeepSDF: Learning continuous signed distance functions for shape representation. In *Proceedings of the IEEE/CVF conference on computer vision and pattern recognition*. 165–174.
- [21] Nasim Rahaman, Aristide Baratin, Devansh Arpit, Felix Draxler, Min Lin, Fred Hamprecht, Yoshua Bengio, and Aaron Courville. 2019. On the spectral bias of neural networks. In *International Conference on Machine Learning*. PMLR, 5301–5310.
- [22] Massimo Selva, Bruno Aiazzi, Francesco Butera, Leandro Chiarantini, and Stefano Baronti. 2015. Hyper-sharpening: A first approach on SIM-GA data. *IEEE J. Sel. Top. Appl. Earth Obs. Remote Sens.* 8, 6 (2015), 3008–3024.
- [23] Tiancheng Shen, Yuechen Zhang, Lu Qi, Jason Kuen, Xingyu Xie, Jianlong Wu, Zhe Lin, and Jiaya Jia. 2022. High quality segmentation for ultra high-resolution images. In *Proceedings of the IEEE/CVF Conference on Computer Vision and Pattern Recognition*. 1310–1319.
- [24] Wenzhe Shi, Jose Caballero, Ferenc Huszar, Johannes Totz, Andrew P Aitken, Rob Bishop, Daniel Rueckert, and Zehan Wang. 2016. Real-time single image and video super-resolution using an efficient sub-pixel convolutional neural network. In *Proceedings of the IEEE conference on computer vision and pattern recognition*. 1874–1883.
- [25] Vincent Sitzmann, Julien Martel, Alexander Bergman, David Lindell, and Gordon Wetzstein. 2020. Implicit neural representations with periodic activation functions. *Advances in Neural Information Processing Systems* 33 (2020), 7462–7473.
- [26] Vincent Sitzmann, Michael Zollhöfer, and Gordon Wetzstein. 2019. Scene representation networks: Continuous 3d-structure-aware neural scene representations. *Advances in Neural Information Processing Systems* 32 (2019).
- [27] Gaochao Song, Luo Zhang, Ran Su, Jianfeng Shi, Ying He, and Qian Sun. 2023. OPE-SR: Orthogonal Position Encoding for Designing a Parameter-free Upsampling Module in Arbitrary-scale Image Super-Resolution. *arXiv preprint arXiv:2303.01091* (2023).
- [28] Jiaxiang Tang, Xiaokang Chen, and Gang Zeng. 2021. Joint implicit image function for guided depth super-resolution. In *Proceedings of the 29th ACM International Conference on Multimedia*. 4390–4399.
- [29] Yuliya Tarabalka, Jocelyn Chanussot, and Jón Atli Benediktsson. 2009. Segmentation and classification of hyperspectral images using minimum spanning forest grown from automatically selected markers. *IEEE Transactions on Systems, Man, and Cybernetics, Part B (Cybernetics)* 40, 5 (2009), 1267–1279.
- [30] Muhammad Uzair, Arif Mahmood, and Ajmal S Mian. 2013. Hyperspectral Face Recognition using 3D-DCT and Partial Least Squares. In *BMVC*, Vol. 1. 10.
- [31] Hien Van Nguyen, Amit Banerjee, and Rama Chellappa. 2010. Tracking via object reflectance using a hyperspectral video camera. In *2010 IEEE Computer Society Conference on Computer Vision and Pattern Recognition-Workshops*. IEEE, 44–51.

- [32] Wu Wang, Weihong Zeng, Yue Huang, Xinghao Ding, and John Paisley. 2019. Deep Blind Hyperspectral Image Fusion. In *ICCV*.
- [33] Yudong Wang, Liang-Jian Deng, Tian-Jing Zhang, and Xiao Wu. 2021. SSconv: Explicit spectral-to-spatial convolution for pansharpening. In *Proceedings of the 29th ACM International Conference on Multimedia*. 4472–4480.
- [34] Qi Xie, Minghao Zhou, Qian Zhao, Zongben Xu, and Deyu Meng. 2022. MHF-net: An interpretable deep network for multispectral and hyperspectral image fusion. *IEEE Transactions on Pattern Analysis and Machine Intelligence* 44 (March 2022), 1457–1473.
- [35] Ting Xu, Tingzhu Huang, Liangjian Deng, and Naoto Yokoya. 2022. An Iterative Regularization Method based on Tensor Subspace Representation for Hyperspectral Image Super-Resolution. *IEEE Trans. Geosci. Remote Sens.* 60 (2022), 1–16. <https://doi.org/10.1109/TGRS.2022.3176266>
- [36] Xingqian Xu, Zhangyang Wang, and Humphrey Shi. 2021. Ultrar: Spatial encoding is a missing key for implicit image function-based arbitrary-scale super-resolution. *arXiv preprint arXiv:2103.12716* (2021).
- [37] Kaiwei Zhang, Dandan Zhu, Xiongkuo Min, and Guangtao Zhai. 2022. Implicit Neural Representation Learning for Hyperspectral Image Super-Resolution. *IEEE Transactions on Geoscience and Remote Sensing* 61 (2022), 1–12.
- [38] Xueting Zhang, Wei Huang, Qi Wang, and Xuelong Li. 2020. SSR-NET: Spatial-spectral reconstruction network for hyperspectral and multispectral image fusion. *IEEE Trans. Geosci. Remote Sens.* 59, 7 (2020), 5953–5965.